Supporting Information

Chemical-physical synergistic etching enabling deep reconstruction of NiFe Prussian blue analogue for efficient oxygen evolution reaction and Zn-air batteries

Luchun Qiu[a]†, Qi Wang[a]†, Ping Yan[b]* and Xin-Yao Yu[a,b]*

[a]Institutes of Physical Science and Information Technology

Anhui University

Hefei 230601, P. R. China

[b]School of Materials Science and Engineering

Anhui University

Hefei 230601, P. R. China

†These two authors contribute equally to this work.

***Corresponding Authors**

*Email: yuxinyao@ahu.edu.cn

*Email: yanping@ahu.edu.cn

Chemicals*:* Nickel chloride hexahydrate ($NiCl_2·6H_2O$), trisodium citrate dehydrate ($C_6H_5Na_3O_7·2H_2O$), potassium hexacyanoferrate(III) ($K_3Fe(CN)_6$), potassium hydroxide (KOH), N,N-dimethylformamide (DMF) and zinc aetate dihydrate ($C_4H_6O_4Zn·2H_2O$) were purchased from Sinopharm Chemical Reagent. Nickel nitrate hexahydrate ($NiN_2O_6·6H_2O$), Pt/C, and RuO_2 were purchased from Macklin. All purchased chemicals were not further purified and all solvents were analytical grade.

Synthesis of NiFe NCs**:** NiFe NCs were synthesized by precipitation method. In a typical synthesis, 0.33 g of $C_6H_5Na_3O_7·2H_2O$ and 0.143 g of $NiCl_2·6H_2O$ were mixed in 20 mL of deionized water (DIW). 0.132 g of $K_3Fe(CN)_6$ was dissolved in 20 mL of DIW. Then, the two solutions were mixed under continuous magnetic stirring for 2 min and the obtained green mixed solution remained stationary for 24 hours at 25 ℃. After that, the yellow products were centrifuged at 9000 rpm and then washed alternately with DIW and ethanol for more than three times. Finally, the precipitates were dried overnight.

Synthesis of NiFe NBs: In a typical synthesis, 0.03 g of NiFe NCs were dispersed in 30 mL of DMF under stirring for 30 min. Then, the mixture solution was placed in an autoclave and heated at 200 ℃ for 20 hours. When the temperature was cooled down to room temperature, the dark green products were centrifuged at 9000 rpm and then washed alternately with ethanol and DIW for more than three times. Lastly, the precipitates were dried overnight.

Synthesis of P-NiFe NBs: The NiFe NBs were etched by N_2 plasma for 10 min with the plasma power of 300 W and gas pressure of 60 Pa. For comparison, the NiFe NBs were also etched by plasma with etching time of 5 min and 15 min and denoted as P-NiFe NBs-5min and P-NiFe NBs-15min.

Synthesis of P-NiFe NCs: The plasma etching process is similar to that of P-NiFe NBs, except using NiFe NCs as the precursors.

Material characterizations*:* The morphologies and elemental contents of the obtained

samples were characterized by using SEM instrument with EDX (Zeiss sigma 500) and TEM instrument (FEI Tecnai G2 F20). The XRD patterns were collected on PANalytical Empyrean. The XPS spectra were analyzed on Thermo Fischer ESCALAB 250 Xi. The *in-situ* Raman spectra were collected by BWS415-7855 i-Raman. The pre-catalysts are loaded on Ni foam. The laser spot with a wavelength of 785 nm was directed on Ni foam. The LSV tests were carried out at the voltage ranging from open circuit potential to 1.58 V (vs. RHE) at a scan rate of 0.5 mV s^{-1}, during which the Raman spectra were recorded simultaneously. The FTIR were performed by Vertex80+Hyperion2000. The ion chromatographic curves were measured by ICS-3000.

Electrochemical characterizations: All the electrochemical measurements were carried out by using CHI 760E at room temperature. 1.0 M KOH electrolyte was used. Graphite rod was served as counter electrode and Hg/HgO electrode was employed as reference electrode. All potentials were given with respect to the reversible hydrogen electrode (RHE): E (*vs.* RHE) = E (*vs.* Hg/HgO) + 0.098 V + 0.0592 × pH.

The catalyst ink was prepared by dispersing 5 mg of catalyst in the mixture of 270 μL of ethanol, 200 μL of deionized water, and 30 μL of Nafion solution (5 wt %) with sonication for 30 min. After that, 2.5 μL of uniformly dispersed catalyst ink was dropped onto the RDE. The loading of catalysts on RDE was 0.35 mg cm^{-2}. Finally, the RDE was dried at room temperature for further characterization. The RDE was rotated at 1600 rpm to eliminate the resulting oxygen bubble during electrocatalytic tests. All the LSV curves were measured at 5 mV s^{-1} and were corrected by 90% iR-compensation. The C_{dl} method was used to estimate the ECSA. As for C_{dl}, it was acquired by cyclic voltammetry method at different scanning rates between 0.82 and 0.92 V *vs.* RHE (20-120 mV s^{-1}). The differences of current densities at 0.87 V were plotted as a function of scan rates. The slope of the fitted line was equal to half of the C_{dl}. The EIS tests were collected at an amplitude of 5 mV as well as frequency range of 10^5~0.1 Hz. When Ni foam is used as the support, the loading of catalysts on Ni foam was

around 1 mg cm^{-2}. The stability of the catalysts was evaluated by CA method at a constant potential.

The TOF could be calculated by the following formula:

$$TOF = \frac{1}{x \cdot n \cdot F}$$

Where *I* is the current density at a specific overpotential, *x* refers to the number of electrons transfer, *F* is the Faraday constant (96485 C mol^{-1}), and *n* represents the amount of moles of active sites (including Ni and Fe).

The FE for OER was determined by rotating ring-disk electrode. The generated O_2 molecules were detected by oxygen reduction reaction when the ring potential was 0.4 V. The FE value of O_2 was calculated using the following formula:

$$FE = \frac{I_{ring}}{I_{disk} \cdot C_e}$$

Where I_{ring} means the ring current, I_{disk} refers to the disk current, and C_e represents the collection efficiency (here is 0.424).

Assembly of aqueous ZABs*:* The homemade ZAB was assembled by polished Zn plate anode, air cathode, and electrolyte. The polished Zn plate was served as anode. The electrolyte is consisted of 6 M KOH and 0.2 M $C_4H_6O_4Zn{\cdot}2H_2O$ to ensure reversible zinc electrochemical reactions at the Zn anode. 20 mg mixture of NiOOH/FeOOH NBs and Pt/C (mass ratio of 1:1) was dispersed in 652 μL of ethanol, 261 μL of deionized water, and 87 μL of Nafion solution (5 wt%) and then the resulting mixture was sonicated for 1 hour to form a homogenous ink. The resulting ink was applied dropwise to a water-repellent carbon paper, dried naturally, and then used as the air cathode catalyst. The mass loading of catalysts was 4.0 mg cm^{-2}.

Assembly of flexible ZABs*:* The flexible ZAB was fabricated with a polished Zn foil anode, mixture of NiOOH/FeOOH NBs and Pt/C as air cathode catalyst, and polyvinyl alcohol (PVA) as electrolyte. The gel electrolyte was prepared as following: 1.0 g of PVA powder

(1799) was added into 10 mL of DIW; the mixture was stirred at 100 ℃ for 30 min and then 3 mL of 18 M KOH with 0.02 M zinc acetate was added into the mixture at 100 ℃; after being stirred for 2 h, the gel was poured into container, freezed at -5 ℃ for 2 h, and thawed at room temperature.

ZABs tests: All ZABs were tested under ambient atmosphere at 25 ℃. The polarization curve measurements were performed by linear sweep voltammetry (5 mV s^{-1}) with CHI 760 E electrochemical working station (CH Instrument). The power density (P) is calculated based on the discharge curve using the following equation: $P = U \times j$, where U is the discharge voltage and j is the discharge current density. The Galvanostatic charge-discharge cycling tests were conducted using a recurrent galvanic pulse method with each cycle being 20 min (10 min for discharge followed with 10 min for charge) for aqueous batteries and 10 min for flexible batteries (5 min for discharge followed with 5 min for charge). The specific capacities were determined by the galvanostatic discharge results, normalized to the mass of consumed Zn. The energy efficiency (EF) is calculated using the following equation:

$$EF = \frac{E_{discharge}}{E_{charge}} \times 100\% = \frac{U_{discharge}}{U_{charge}} \times 100\%$$

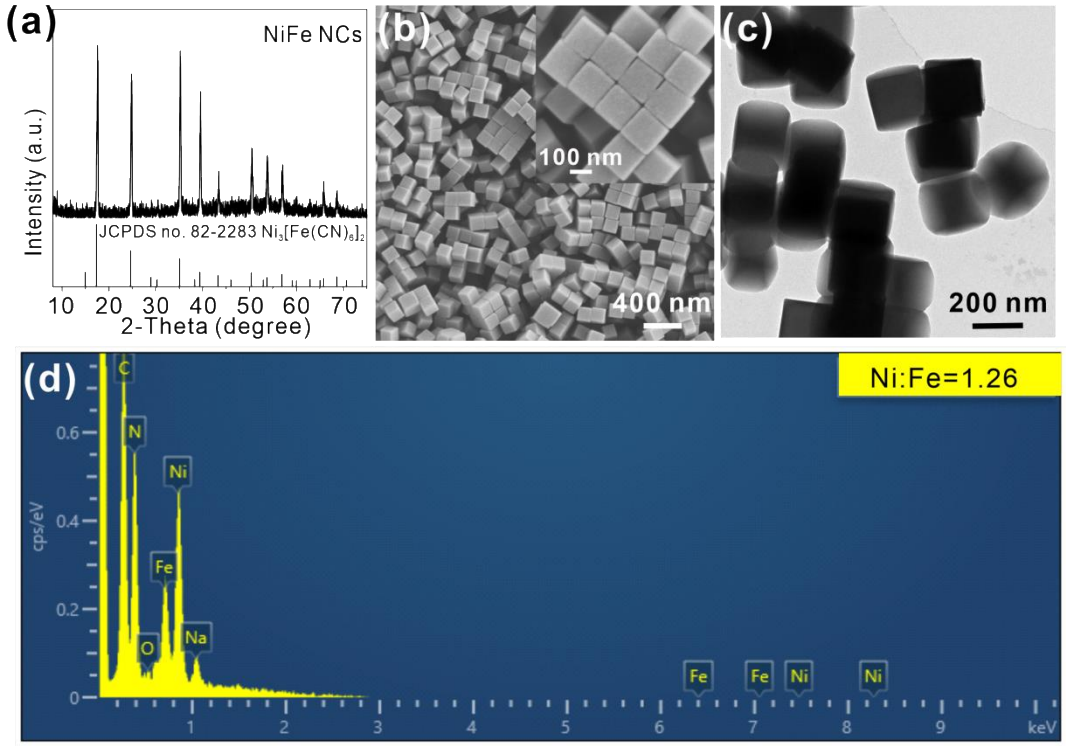

Fig. S1. (a) XRD pattern, (b) SEM images, (c) TEM image, and (d) EDX spectrum of NiFe NCs.

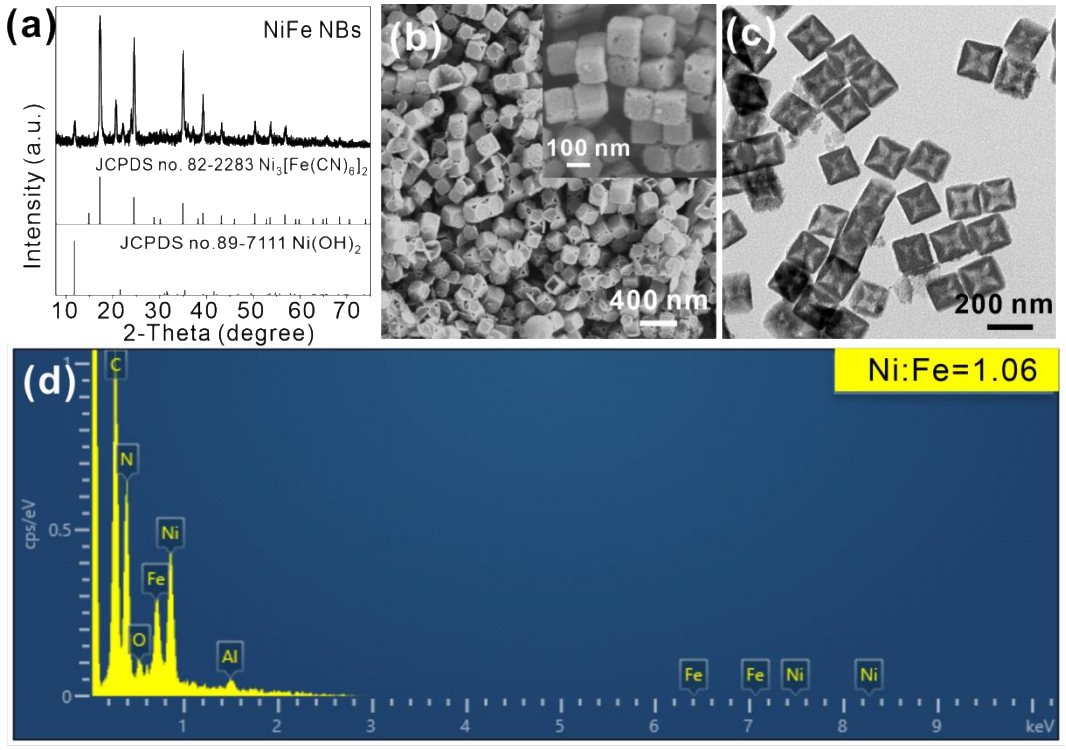

Fig. S2. (a) XRD pattern, (b) SEM images, (c) TEM image, and (d) EDX spectrum of NiFe NBs.

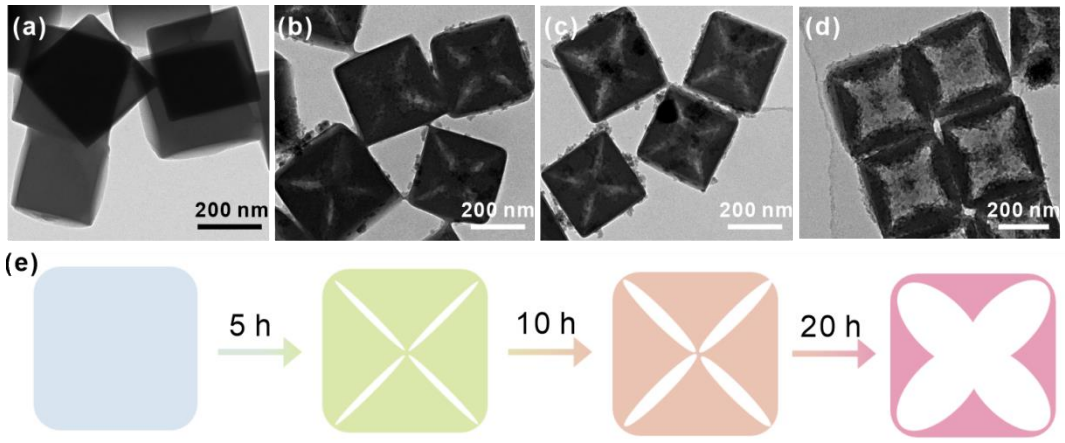

Fig. S3. TEM images of the samples collected in the chemical etching process at 0 h (a), 5 h (b), 10 h (c), and 20 h (d). (e) Schematic illustration for the chemical etching process.

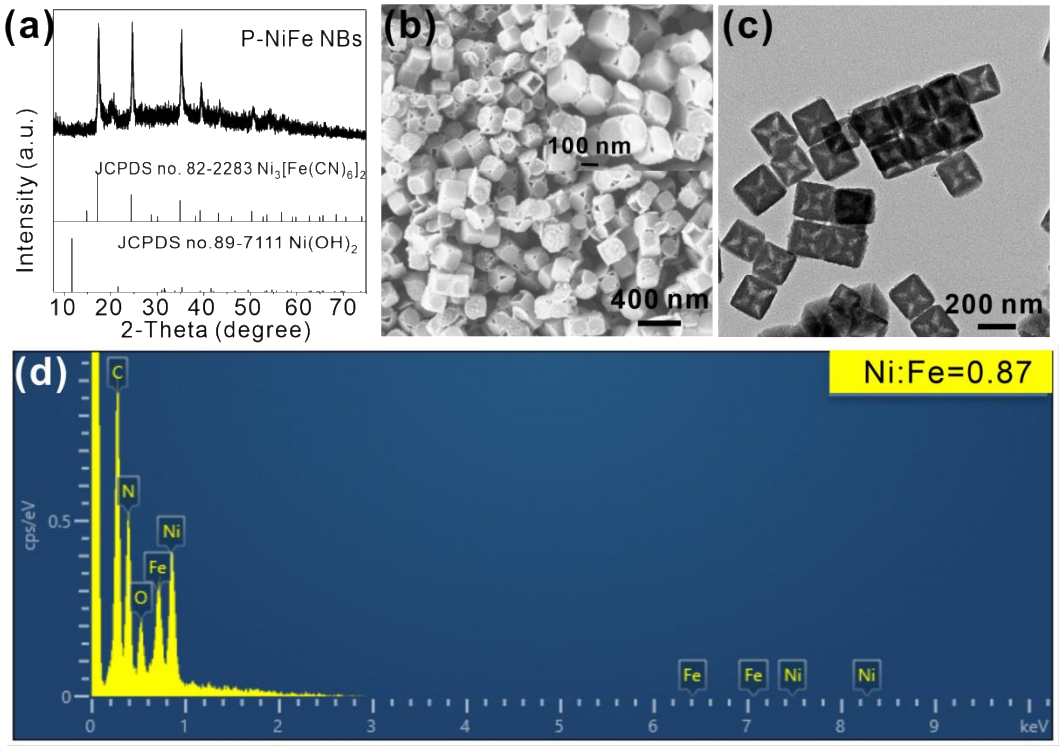

Fig. S4. (a) XRD pattern, (b) SEM images, (c) TEM image, and (d) EDX spectrum of P-NiFe NBs.

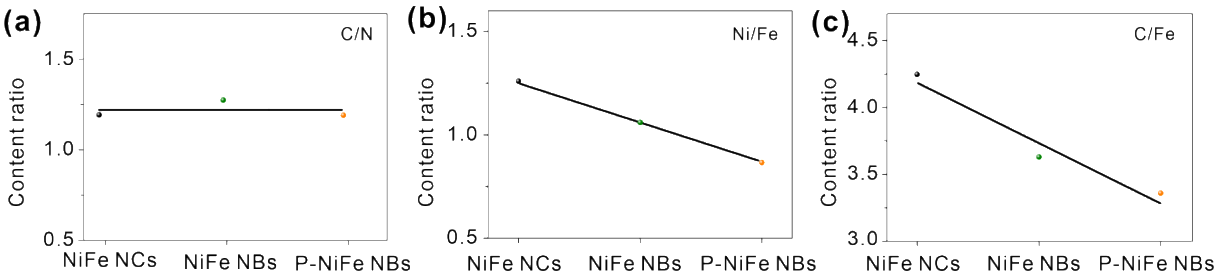

Fig. S5. The elemental ratios of C/N (a), Ni/Fe (b), and C/Fe (c) of NiFe NCs, NiFe NBs, and P-NiFe NBs determined from EDX spectra.

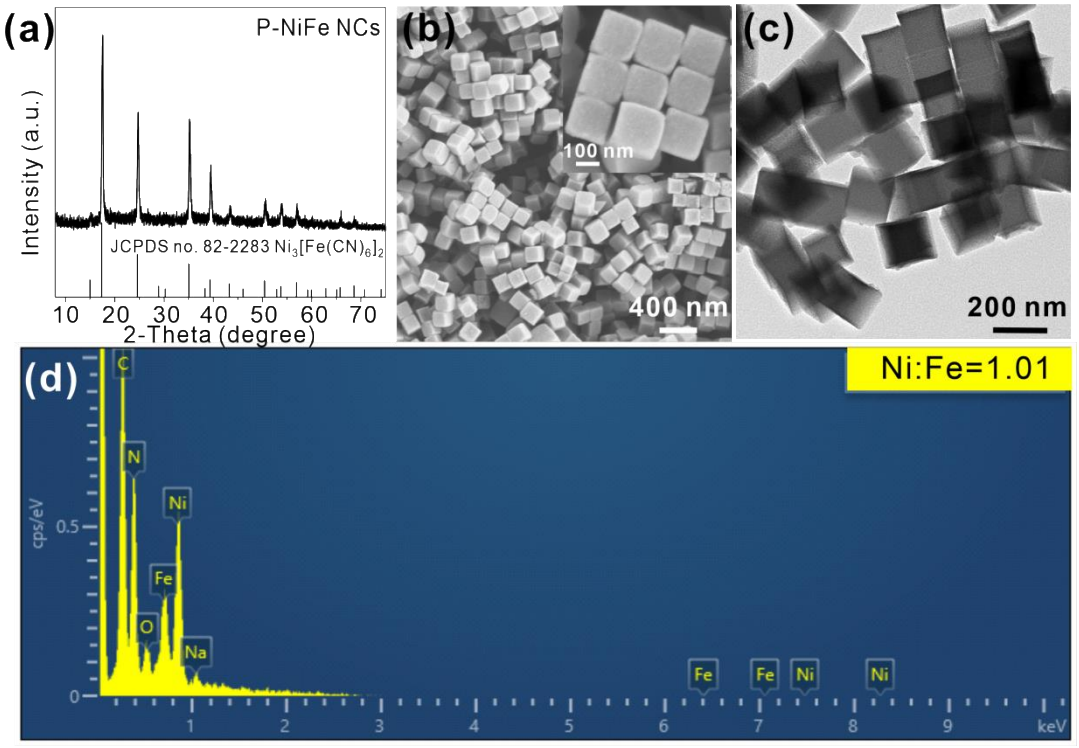

Fig. S6. (a) XRD pattern, (b) SEM images, (c) TEM image, and (d) EDX spectrum of P-NiFe NCs.

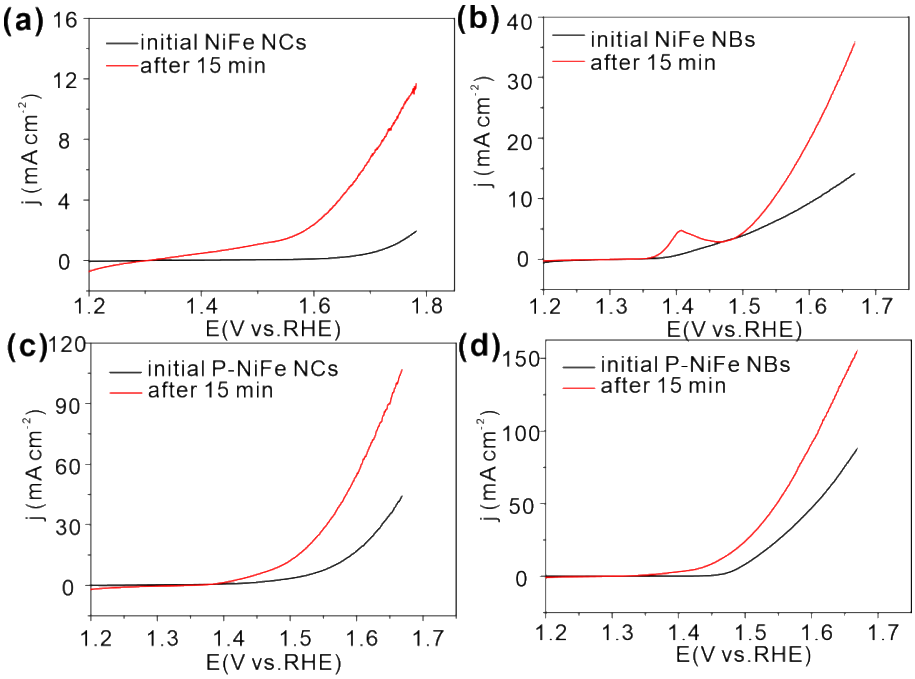

Fig. S7. LSV curves of NiFe NCs (a), NiFe NBs (b), P-NiFe NCs (c), and P-NiFe NBs on RDE before and after CA test at 1.59 V *vs.* RHE.

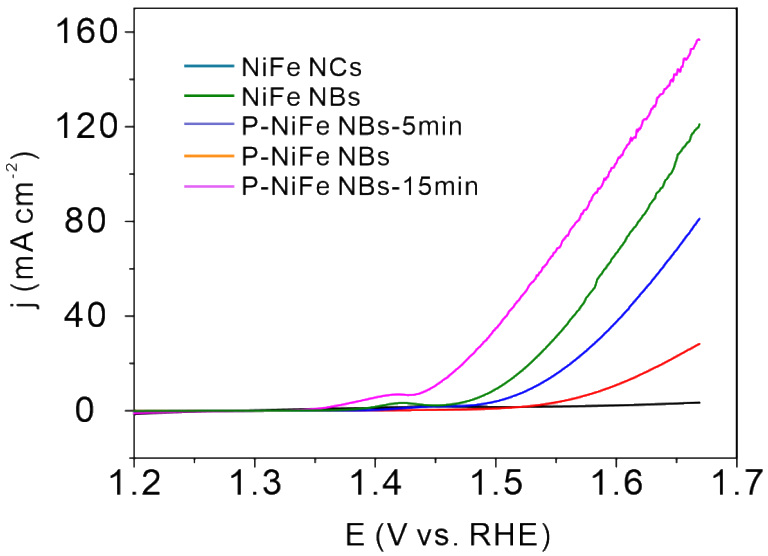

Fig. S8. LSV curves of NiFe NCs, NiFe NBs, P-NiFe NBs-5 min, P-NiFe NBs (etching time of 10 min), and P-NiFe NBs-15min on RDE after CA test at 1.59 V *vs.* RHE.

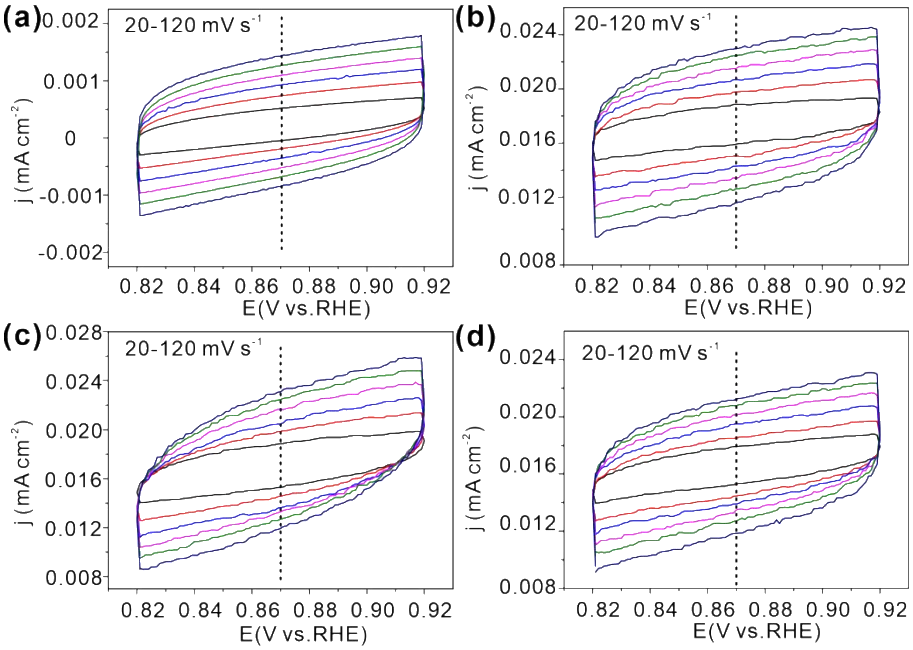

Fig. S9. CV curves of NiFe NCs (a), NiFe NBs (b), NiFe NCs (c), and P-NiFe NBs (d) at different scan rates from 20 to 120 mV s^{-1}.

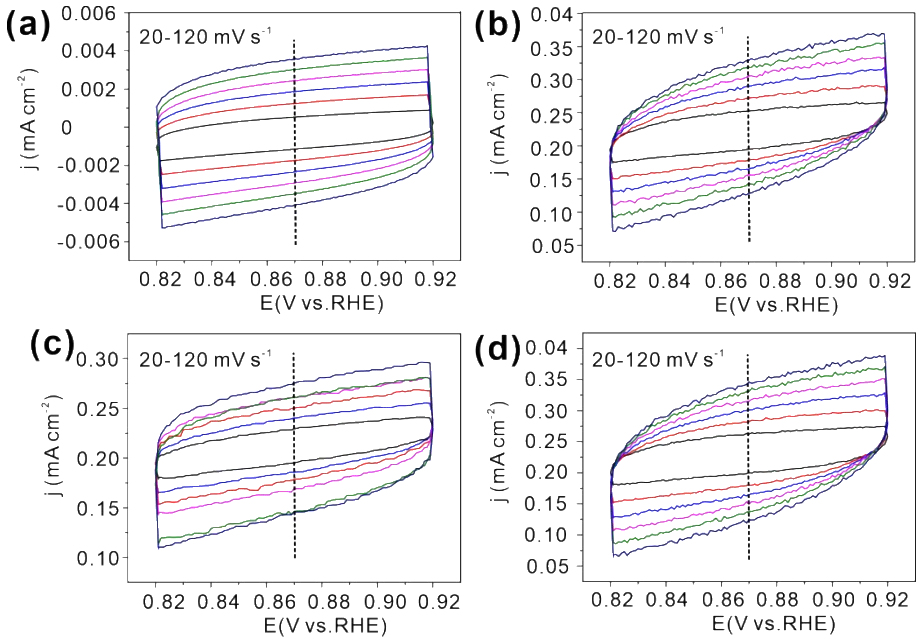

Fig. S10. CV curves of Re-NiFe NCs (a), Re-NiFe NBs (b), Re-P-NiFe NCs (c), and Re-P-NiFe NBs (d) at different scan rates from 20 to 120 mV s^{-1}.

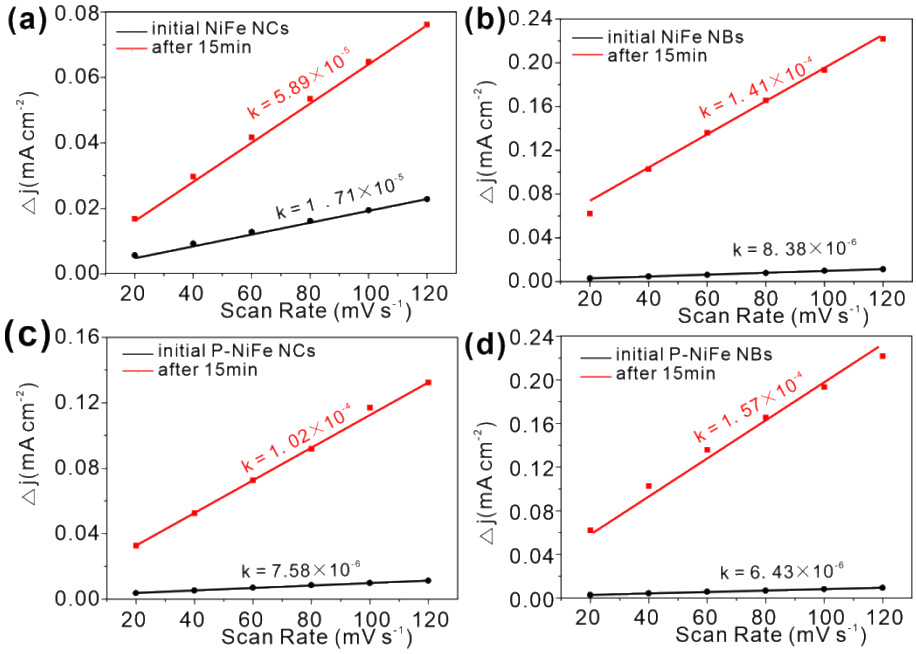

Fig. S11. Current density differences ($\triangle j$) of NiFe NCs (a), NiFe NBs (b), P-NiFe NCs (c), and P-NiFe NBs (d) before and after reconstruction as a function of scan rate.

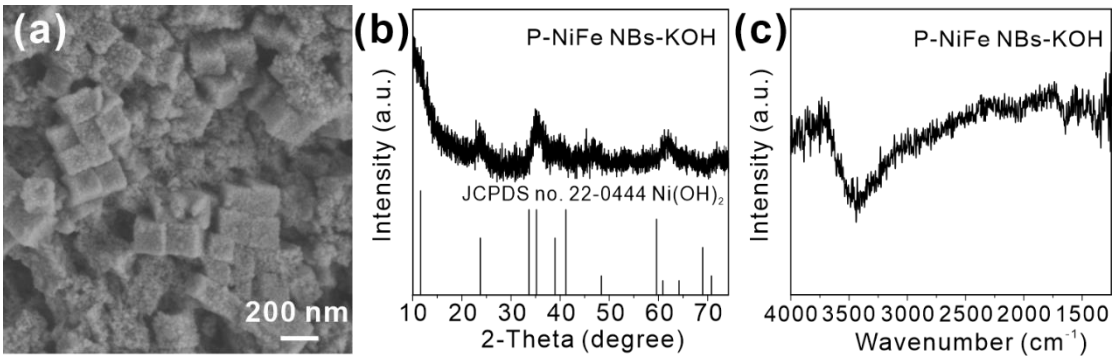

Fig. S12. (a) SEM image, (b) XRD pattern, and (c) FTIR spectrum of P-NiFe NBs after soaking in 1 M KOH for one day.

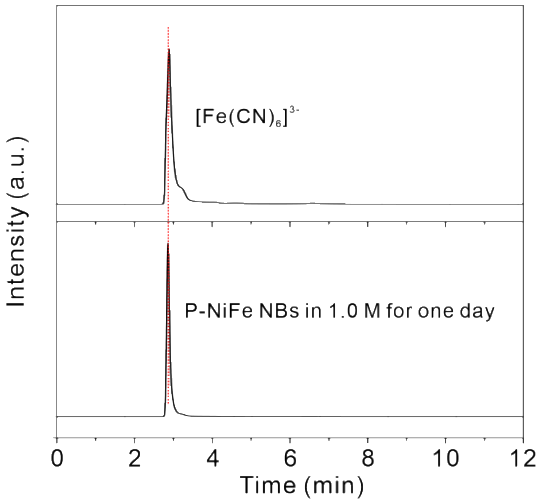

Fig. S13. IC curves of prepared potassium ferricyanide solution (up) and the solution collected after soaking the P-NiFe NBs in 1 M KOH for one day (bottom).

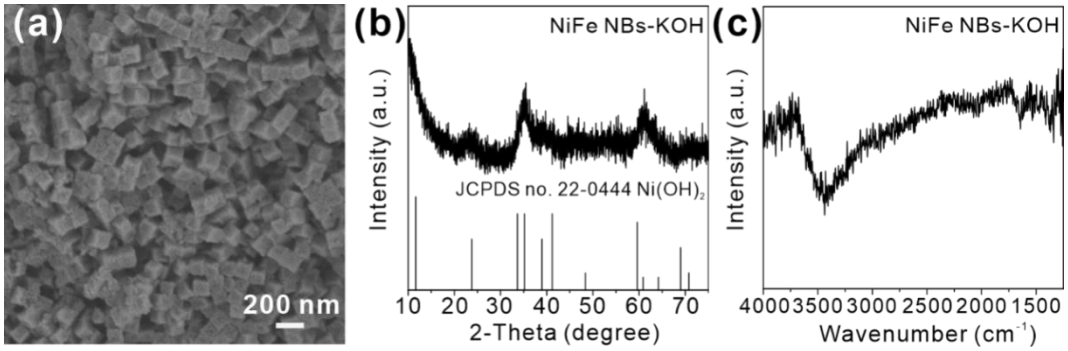

Fig. S14. (a) SEM image, (b) XRD pattern, and (c) FTIR spectrum of NiFe NBs after soaking in 1 M KOH for one day.

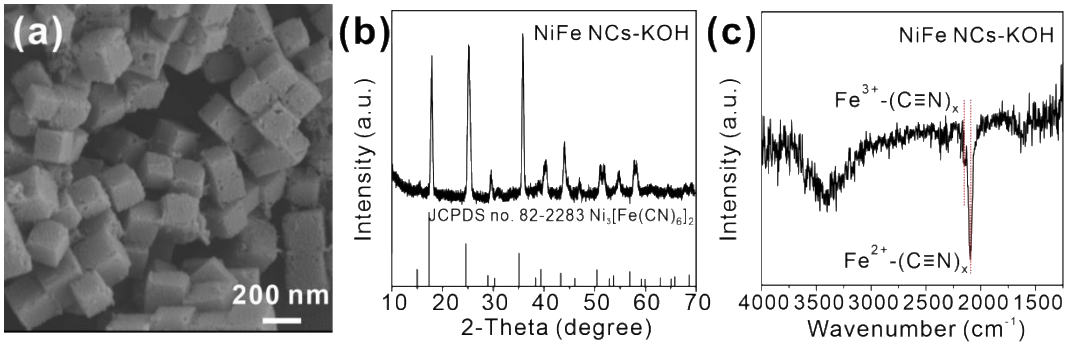

Fig. S15. (a) SEM image, (b) XRD pattern, and (c) FTIR spectrum of NiFe NCs after soaking in 1 M KOH for one day.

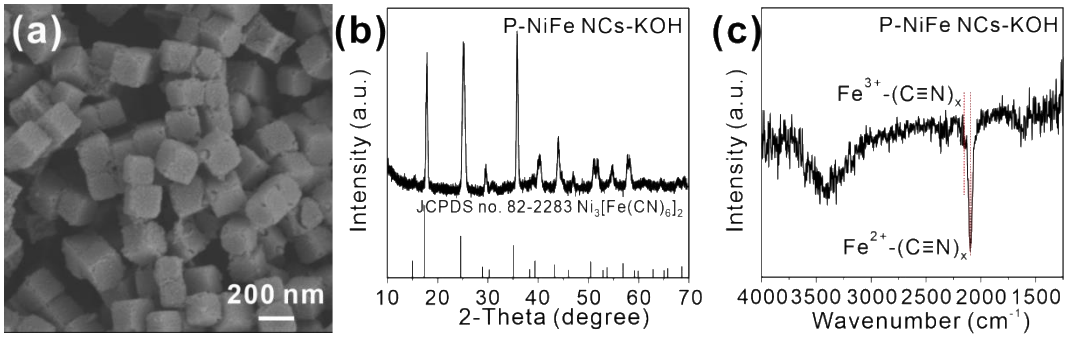

Fig. S16. (a) SEM image, (b) XRD pattern, and (c) FTIR spectrum of P-NiFe NCs after soaking in 1 M KOH for one day.

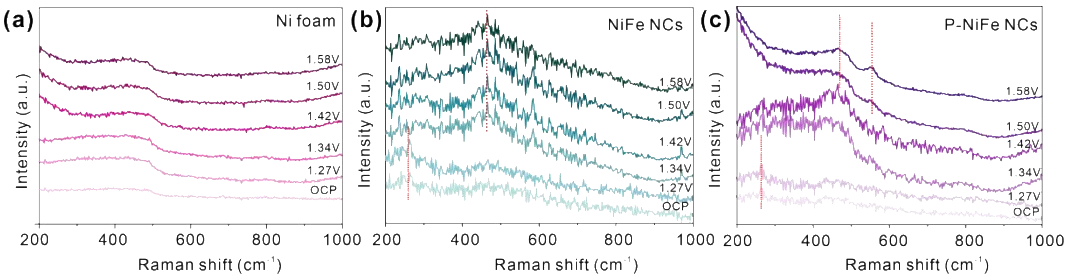

Fig. S17. In-situ Raman spectra of (a) Ni foam, (b) NiFe NCs, and (c) P-NiFe NCs at various potentials.

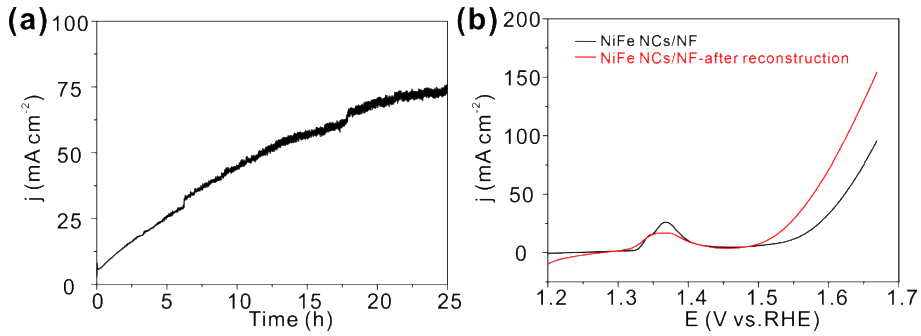

Fig. S18. (a) CA test of NiFe NCs on Ni foam for 30 h at 1.82 V *vs.* RHE and (b) LSV curves of NiFe NCs before and after reconstruction.

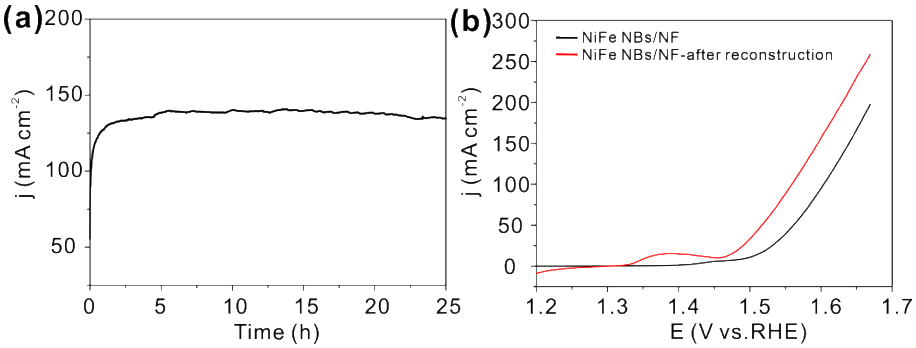

Fig. S19. (a) CA test of NiFe NBs on Ni foam for 30 h at 1.82 V *vs.* RHE and (b) LSV curves of NiFe NBs before and after reconstruction.

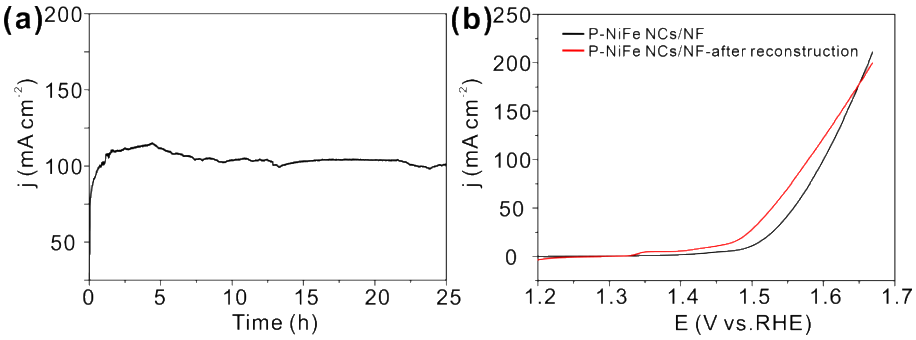

Fig. S20. (a) CA test of P-NiFe NCs on Ni foam for 30 h at 1.82 V *vs.* RHE and (b) LSV curves of P-NiFe NCs before and after reconstruction.

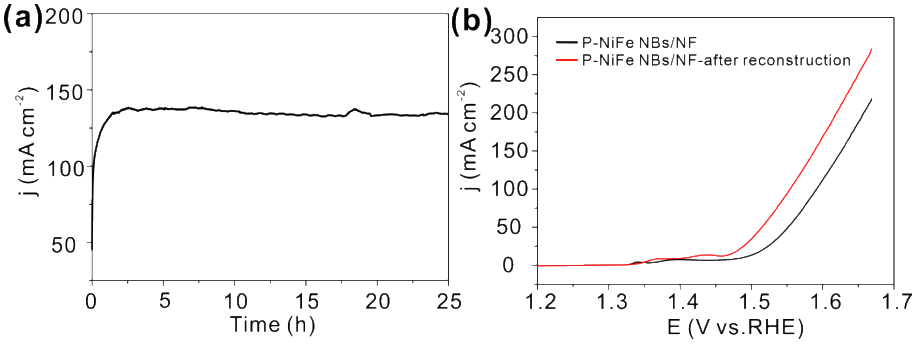

Fig. S21. (a) CA test of P-NiFe NBs on Ni foam for 30 h at 1.82 V *vs.* RHE and (b) LSV curves of P-NiFe NBs before and after reconstruction.

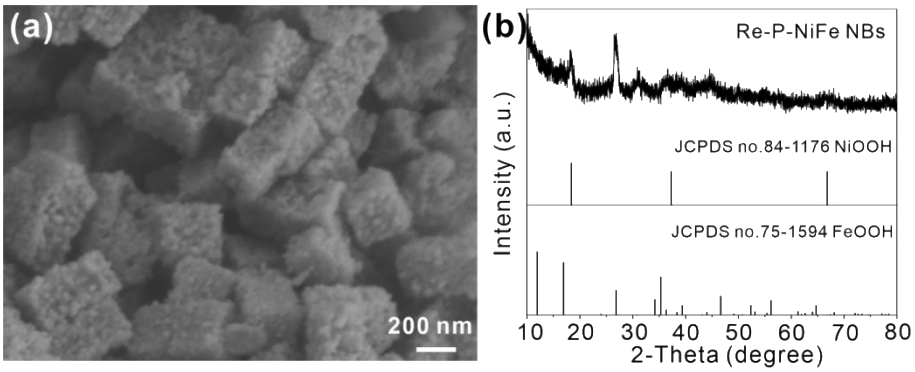

Fig. S22. (a) SEM image and (b) XRD pattern of Re-P-NiFe NBs.

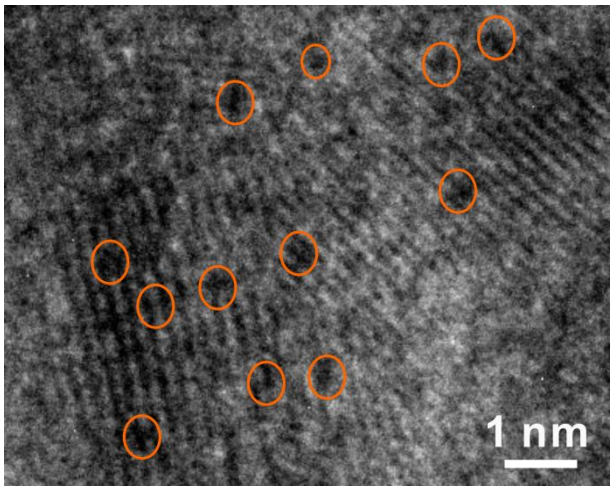

Fig. S23. HRTEM images of Re-P-NiFe NBs.

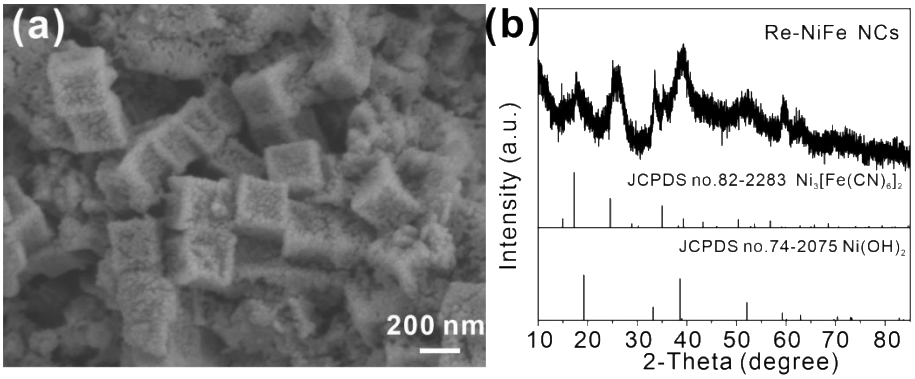

Fig. S24. (a) SEM image and (b) XRD pattern of Re-NiFe NCs.

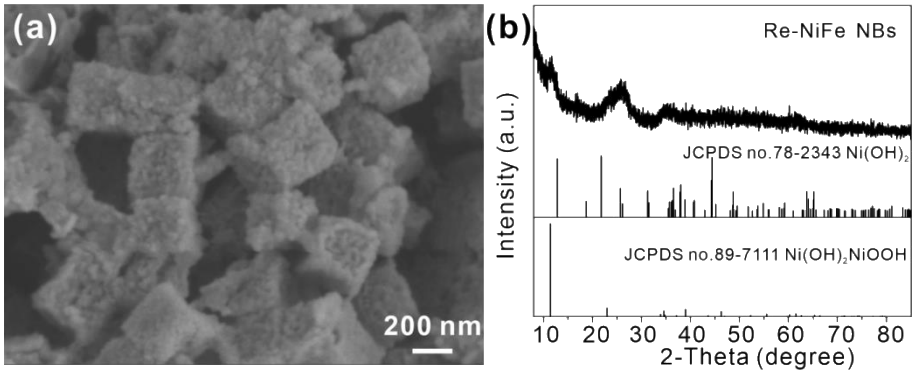

Fig. S25. (a) SEM image and (b) XRD pattern of Re-NiFe NBs.

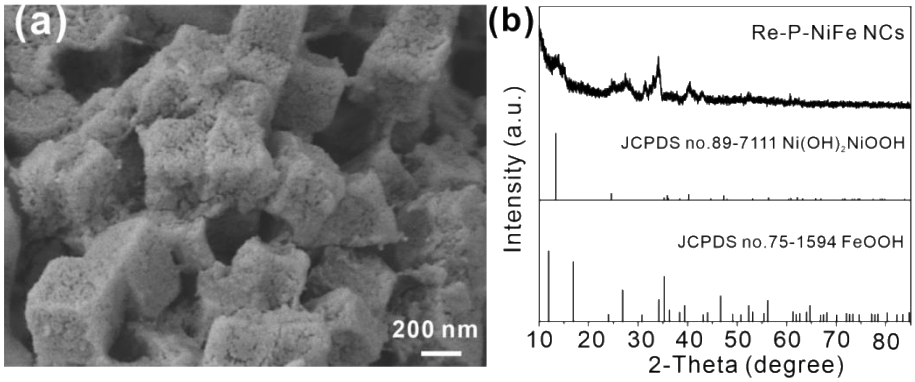

Fig. S26. (a) SEM image and (b) XRD pattern of Re-P-NiFe NCs.

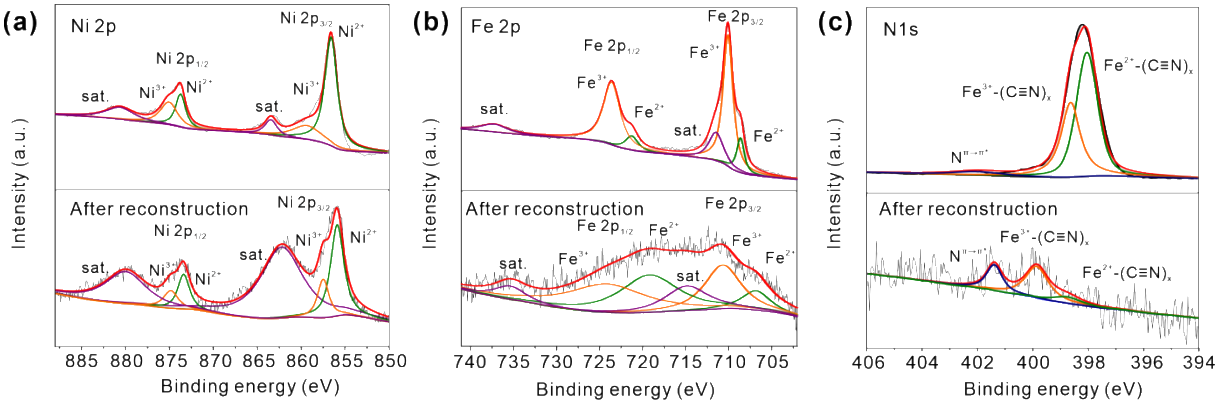

Fig. S27. The Ni 2p (a), Fe 2p (b), and N 1s (c) high-resolution XPS spectra of NiFe NCs and Re-NiFe NCs.

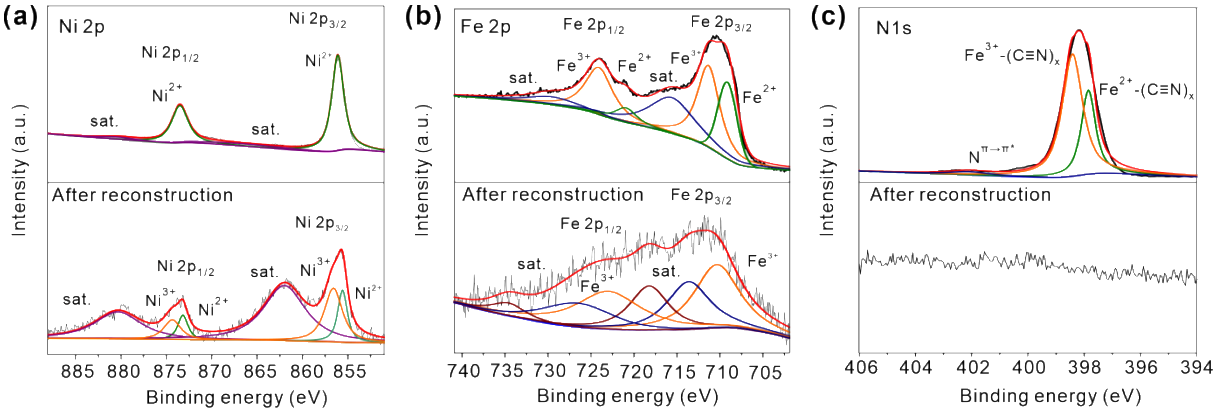

Fig. S28. The Ni 2p (a), Fe 2p (b), and N 1s (c) high-resolution XPS spectra of NiFe NBs and Re-NiFe NBs.

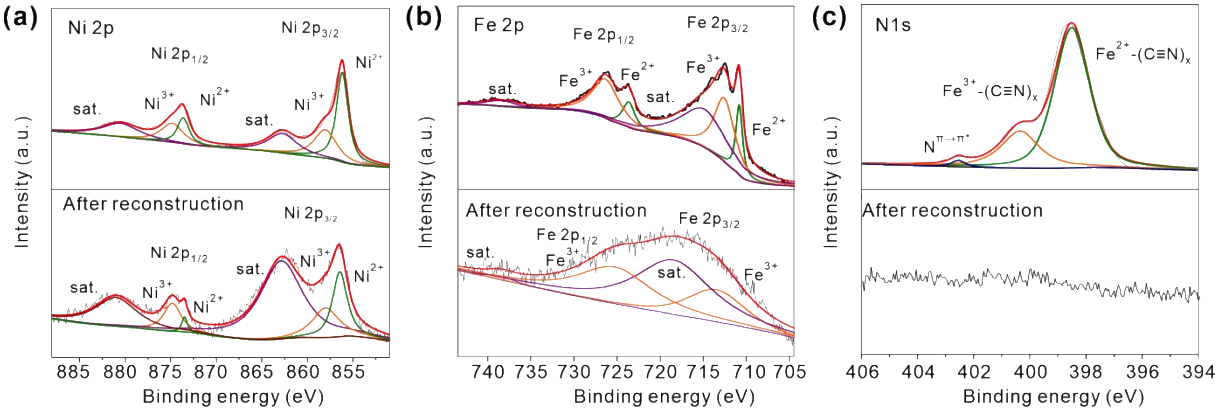

Fig. S29. The Ni 2p (a), Fe 2p (b), and N 1s (c) high-resolution XPS spectra of P-NiFe NCs and Re-P-NiFe NCs.

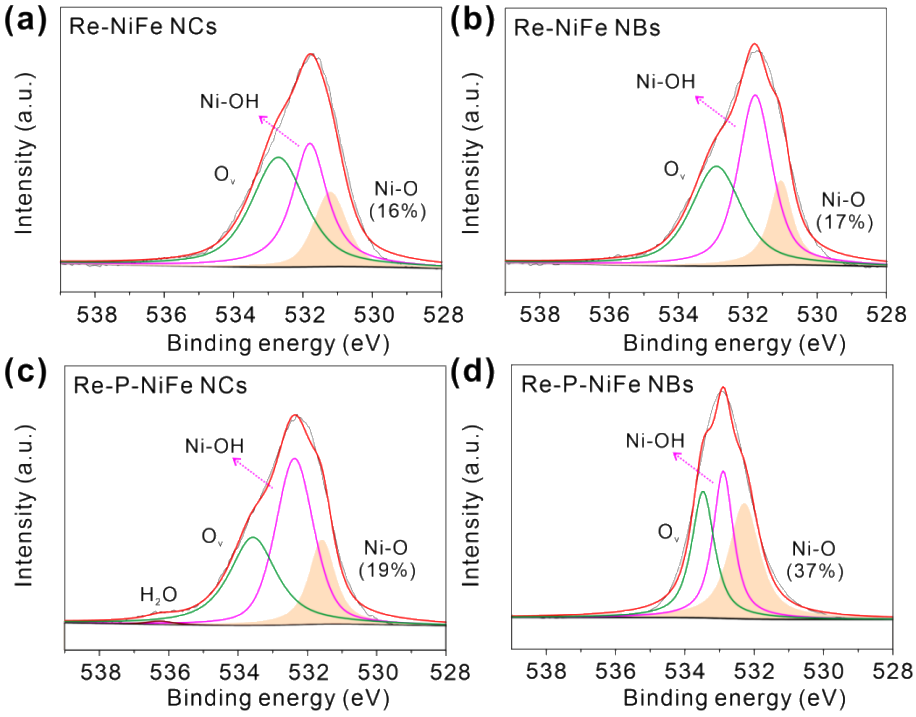

Fig. S30. The O 1s high-resolution XPS spectra of Re-NiFe NCs (a), Re-NiFe NBs (b), Re-P-NiFe NCs (c), and Re-P-NiFe NBs (d).

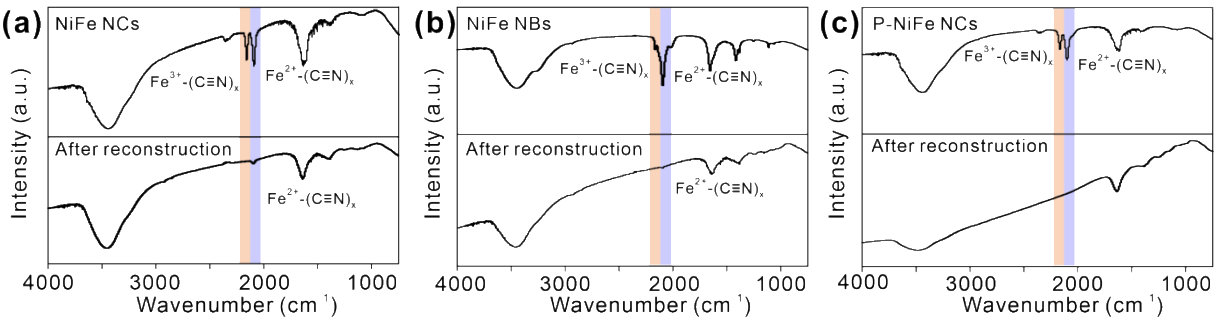

Fig. S31. FT-IR spectra of NiFe NCs/Re-NiFe NCs (a), NiFe NBs/Re-NiFe NBs (b), and P-NiFe NCs/Re-P-NiFe NCs (c).

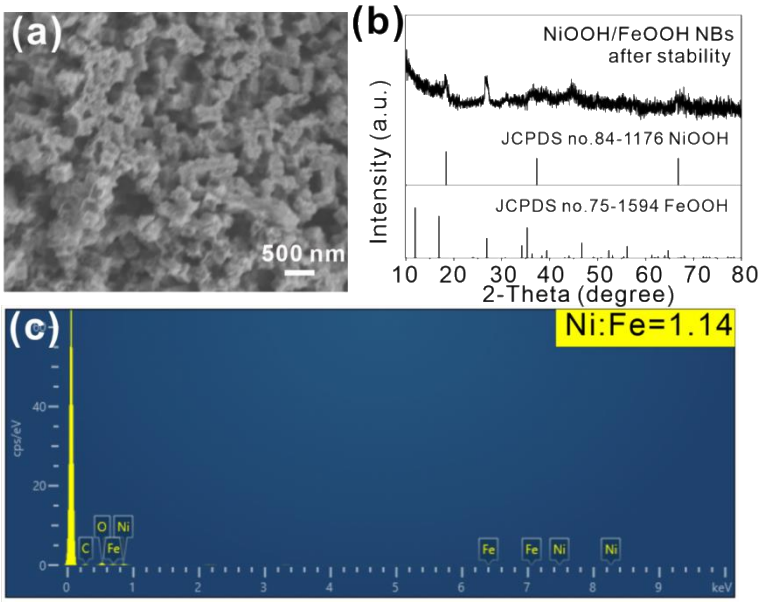

Fig. S32. (a) Large-scale SEM image, (b) XRD pattern, and (c) EDX spectrum of NiOOH/FeOOH NBs after OER stability test.

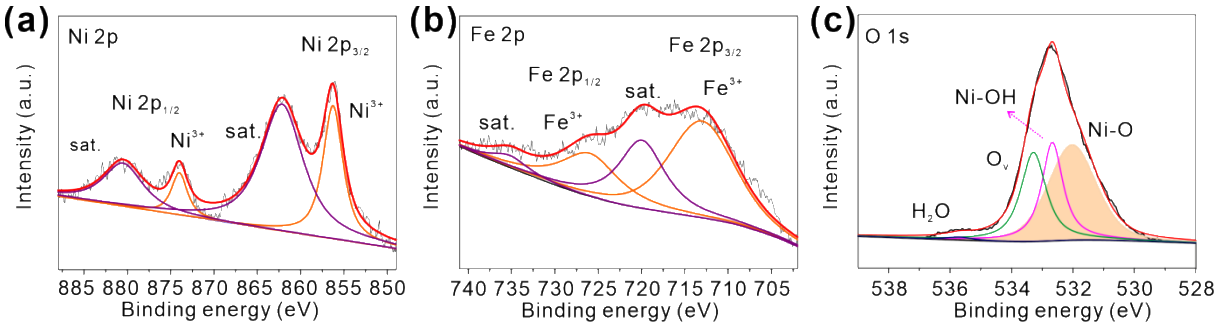

Fig. S33. The Ni 2p (a), Fe 2p (b), and N 1s (c) high-resolution XPS spectra of NiOOH/FeOOH NBs after stability test.

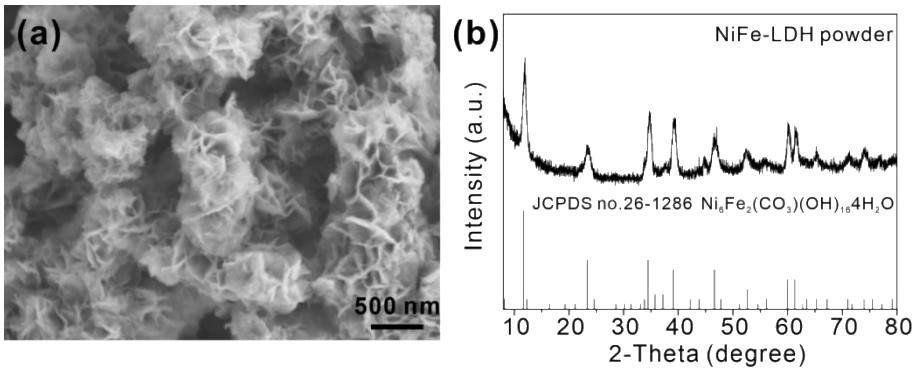

Fig. S34. (a) SEM image and (b) XRD pattern of NiFe LDH.

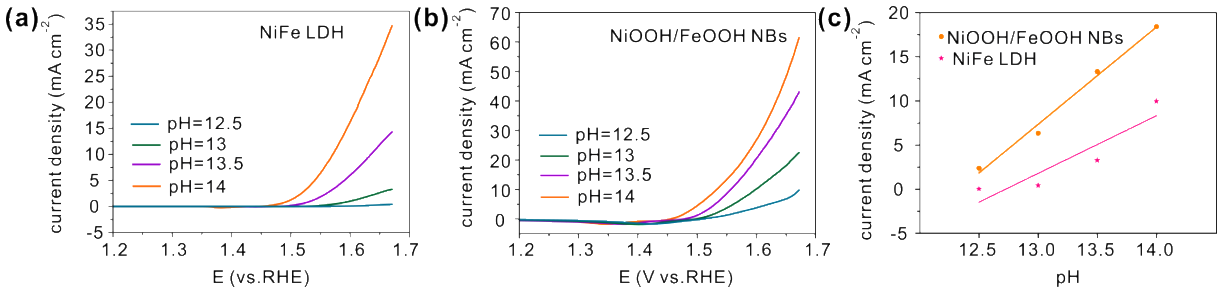

Fig. S35. LSV plots of NiFe LDH (a) and NiOOH/FeOOH NBs (b) measured in KOH with pH from 12.5 to 14; (c) Specific OER activity at 1.57 V *vs.* RHE as a function of pH.

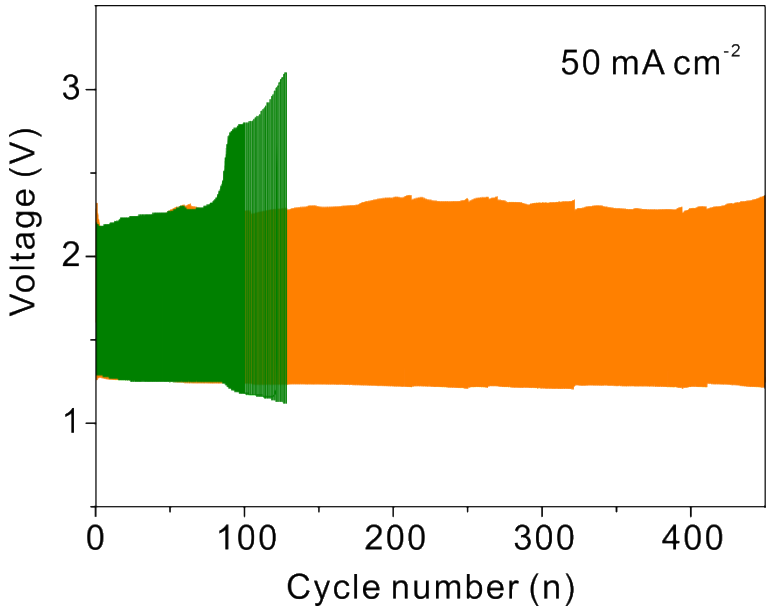

Fig. S36. Charge–discharge stability at 50 mA cm^{-2} of liquid ZABs based on NiOOH/FeOOH NBs + Pt/C and RuO_2 + Pt/C.

Table S1 Comparisons for the OER overpotential of NiOOH/FeOOH NBs on RDE and Ni foam with that of other reported catalysts in 1 M KOH.

Catalyst	Overpotentials on RDE (mV)	Overpotentials on Ni foam (mV)		Ref.
	10 mA cm^{-2}	10 mA cm^{-2}	100 mA cm^{-2}	
NiOOH/FeOOH NBs	**220**	**216**	**270**	**This Work**
Fe_3O_4/FeS_2	253			[1]
Ni-MOF@Fe-MOF	265			[2]
D-RuO_2/TiO_2/TM		296		[3]
$Ni_3Fe_1O_x$@C-800	264			[4]
$MnOOH@CDs_{0.2}$	302			[5]
MoS_2/NiS–Ni_3S_2/NF			460	[6]
IrO_2@SL-NiFe LDHs		270		[7]
FeCo-LDH/MXene		268		[8]
AlCrCuFeNi HEAs	270			[9]
$NiFe(OH)_x/Ni_3N$		260	290	[10]
NiO-Ni/NF			323	[11]
FeOOH@Co@FeOOH HNTAs-NF			310	[12]

Reference

[1] M.J. Wang, X. Zheng, L. Song, X. Feng, Q. Liao, J. Li, L. Li and Z. Wei, *J. Mater. Chem. A* 2020, **8**, 14145.

[2] K. Rui, G.Q. Zhao, Y.P. Chen, Y. Lin, Q. Zhou, J.Y. Chen, J.X. Zhu, W.P. Sun, W. Huang and S. X. Dou, *Adv. Funct. Mater* 2018, **28**, 1801554.

[3]W.Q. Li, H. Zhang, M.Z. Hong, L.L. Zhang, X. Feng, M.F. Shi, W.X. Hua and S.C. Mu, *Chem. Eng. J.* 2022, **431**, 134072.

[4] X. Bai, Y.Y. Ma, Q. Wanga and J.Q. Guan, *Int. J. Hydrogen Energy*, 2022, **47**, 2304.

[5] L. Tian, X. Zhai, X. Wang, X. Pang, J. Li and Z. Li, *Electrochimi. Acta* 2020, **337**, 135823.

[6] Y.Y. Guan, H.C. Xuan, H.S. Li and P.D. Han, *Electrochimi. Acta* 2019, **320**,134614.

[7] D. Li, T. Li, G. Hao, W. Guo, S. Chen, G. Liu, J. Li and Q. Zhao, *Chem. Eng. J.* 2020, **399**, 125738.

[8] M. Tian, Y. Jiang, H. Tong, Y. Xu and L. Xia, *ChemNanoMat* 2019, **6**, 154.

[9] L.H. Liu, N. Li, M. Han, J.R. Han and H.Y. Liang, *Rare Metals* 2021, **41**, 125.

[10] H.J. Zhang, X.F. Meng, J.F. Zhang and Y. Huang, *ACS Sustainable Chem. Eng.* 2021, **9**, 12584.

[11] Z.H. Yue, W.X. Zhu, Y.Z. Li, Z.Y. Wei, N. Hu, Y.R. Suo, and J.L. Wang, *Inorg. Chem.* 2018, **57**, 4693.

[12] J.X. Feng, H. Xu, Y.T. Dong, S.H. Ye, Y.X. Tong and G.R. Li, *Angew. Chem.* 2016, **128**, 3758.